Transition Bars during Transformation of an Amorphous Calcium Carbonate Precursor

Lijun Dai, Xingguo Cheng, and Laurie B. Gower*

Department of Materials Science and Engineering, University of Florida, Gainesville, Florida 32611

Received March 14, 2008. Revised Manuscript Received June 3, 2008

A variety of calcium carbonate ($CaCO_3$) biominerals are now thought to be formed via an amorphous precursor pathway. Our group has been using in vitro model systems to examine potential crystallochemical reactions that might occur during biomineralization and, in particular, has proposed that a polymer-induced liquid-precursor (PILP) mineralization process may play a fundamental role in biomineralization. The PILP process is induced with polyanionic polypeptides (containing aspartic acid and phosphoserine) to produce colloids of an amorphous mineral that are so highly hydrated that they coalesce into smooth mineral films. In situ observations, however, show that these films are not smooth throughout the reaction because transition bars form ridges in the tablets/films as the amorphous phase crystallizes. Using fluorescently labeled polymer, it was determined that the transition bars are due to exclusion of the polymeric impurity into diffusion limited zones as crystallization proceeds across the amorphous phase. There is also evidence to suggest that the excluded polymer may stimulate a secondary deposition of PILP phase that fills in the valleys and ridges to produce a smooth mineral film. These transition bars, which result in anisotropic exclusion of polymer along well-defined crystallographic zones, may be relevant toward understanding the anisotropy of crystal texture in biominerals with occluded proteins.

Introduction

Biologically formed minerals often exhibit complex non-equilibrium morphologies and compositions, unlike geological or synthetic $CaCO_3$, which typically form the common rhombohedral habit of calcite, or spherulitic pin-cushion morphology of aragonite. For example, the aragonite phase found in mollusk nacre is organized into towers of layered tablets (columnar nacre) or in nanolaminated sheets (sheet nacre).[1] The spine of a sea urchin has an even more elaborate morphology consisting of microporous channels of a bicontinuous network of Mg-bearing calcite.[2,3] Interestingly, the spine behaves optically and diffracts as if it were a single crystal of calcite,[4,5] yet has been shown to contain macromolecules (proteins) incorporated within the mineral,[6] making it a single-crystalline composite. This imparts it with unique mechanical properties in that it fractures more like a glass with a conchoidal fracture surface, rather than fracturing along the well-defined cleavage planes of calcite.[7,8]

The incorporated proteins are interesting with respect to the fracture behavior; but they are also of interest to the materials chemist because these water-soluble, mineral associated, acidic (i.e., polyanionic) proteins are thought to modulate the growth of the inorganic crystal during biomineral formation.[9−12] In the older literature, it was proposed that these proteins might preferentially adsorb to specific crystallographic faces, thus modifying the growth kinetics and crystal habit.[12−16] More recently, evidence has been found to suggest that calcific biominerals, such as the urchin spine and mollusk nacre, are formed from an amorphous precursor.[2,17−22] Thus, the hypothesis regarding the role of these polyanionic proteins has shifted to a new paradigm. It

* Corresponding author. E-Mail: lgowe@mse.ufl.edu. Phone: (352) 846-3336. Fax: (352) 846-3355.

(1) Carter, J. G. *Skeletal Biomineralization: Patterns, Processes and Evolutionary Trends*; Van Nostrand Reinhold: New York, 1990; Vol. 1.
(2) Raz, S.; Hamilton, P. C.; Wilt, F. H.; Weiner, S.; Addadi, L. *Adv. Funct. Mater.* **2003**, *13* (6), 480–486.
(3) Tsipursky, S. J.; Buseck, P. R. *Am. Mineral.* **1993**, *78* (7−8), 775–781.
(4) Blake, D. F.; Peacor, D. R.; Allard, L. F. *Micron Microscopica Acta* **1984**, *15* (2), 85–90.
(5) Raup, D. L. The endoskeleton. In Physiology of Echinodermata; Boolootian, R. A., Ed.; Interscience: New York, 1966; pp 379−395.
(6) Berman, A.; Addadi, L.; Weiner, S. *Nature* **1988**, *331*, 546–548.
(7) Weiner, S.; Addadi, L.; Wagner, D. *Mater. Sci. Eng., C* **2000**, *11*, 1–8.
(8) Weber, J.; Greer, R.; Voight, B.; White, E.; Roy, R. *J. Ultrastruct. Res.* **1969**, *26* (5−6), 355–366.
(9) Addadi, L.; Weiner, S. *Proc. Natl. Acad. Sci., U.S.A.* **1985**, *82*, 4110–4114.
(10) Wheeler, A. P.; Sikes, C. S. Matrix-crystal interactions in $CaCO_3$ Biomineralization. In *Biomineralization−Chemical and Biochemical Perspectives*; Mann, S., Webb, J., Williams, R. J. P., Eds.; VCH: New York, 1989; pp 95−131.
(11) Marsh, M. E. Polyanions and Biomineralization. In *Biomineralization 93−7th International Symposium on Biomineralization*, Monaco, Nov 15−16, 1993; Allemand, D., Cuif, J.-P., Eds.; Bulletin de l'Institut Oceanographique: Monaco, 1994; Vol. 14, pp 121−128.
(12) Weiner, S.; Addadi, L. *Trends Biochem. Sci.* **1991**, *16:7*, 252–256.
(13) Addadi, L.; Moradian-Oldak, J.; Weiner, S. Macromolecule-crystal recognition in biomineralization. In *Surface Reactive Peptides and Polymers−Discovery and Commercialization*; Sikes, C. S., Wheeler, A. P., Eds.; ACS Symposium Series 444; American Chemical Society: Washington, D.C., 1991; pp 13−27.
(14) Addadi, L.; Weiner, S. Stereochemical and structural relations between macromolecules and crystals in biomineralization. In *Biomineralization−Chemical and Biochemical Perspectives*; Mann, S., Webb, J., Williams, R. J. P., Eds.; VCH: New York, 1989; pp 133−156.
(15) Addadi, L.; Weiner, S. *Angew. Chem., Int. Ed.* **1992**, *31*, 153–169.
(16) Weiner, S.; Traub, W. *Philos. Trans. R. Soc. London, Ser. B* **1984**, *304*, 425–434.
(17) Addadi, L.; Raz, S.; Weiner, S. *Adv. Mater.* **2003**, *15* (12), 959–970.

10.1021/cm800760p CCC: $40.75
Published on Web 10/29/2008

is now thought that these proteins induce and/or stabilize the amorphous precursor, which allows the mineral to be "molded" within the confines of an insoluble organic matrix or vesicle, generating a variety of species specific, nonequilibrium morphologies.[17] This new hypothesis brings into question the older data that was at the foundation of the former hypothesis, that is, the adsorption of proteins onto specific crystallographic planes. This hypothesis was supported by ex vivo analysis of the crystallographic texture of biominerals (via synchrotron X-ray scattering studies), in which it was suggested that selective adsorption along crystallographically defined planes led to the anisotropic distribution of the occluded proteins.[23−26] The work herein may shed some light on this textural data, upon which much of this former hypothesis was based.

Using in vitro model systems, our group has been examining the influence of polymeric additives on crystal growth, and more specifically, the ability to modulate crystal growth through an amorphous precursor route. In particular, we have found that acidic polypeptides (e.g., peptides enriched with aspartic acid or phosphoserine), which are considered simple mimics to the acidic proteins associated with biominerals, can induce an amorphous $CaCO_3$ phase that is so highly hydrated that it has fluidic character.[27] A fluidic mineral precursor, which initially was a difficult concept to grasp, has now been described by other researchers as well,[28−32] and seems to be gaining more widespread acceptance. We call this process a polymer-induced liquid-precursor (PILP) process because of the important role the acidic polymer plays in generating and stabilizing the fluidic amorphous phase, long enough for it to be molded and shaped into a variety of nonequilibrium morphologies, many of which are strikingly similar to the features found in biominerals (e.g., $CaCO_3$ films and tablets,[27,33,34] similar in morphology to mollusk nacre[35] and bryozoan seminacre,[27] nanofibrous calcite similar to the rods of sea urchin teeth,[36,37] replica of sea urchin spine's bicontinuous microporous network,[38] core−shell particles similar to dinoflagellate cysts,[39] high magnesium-calcite,[40] concentrically laminated spherulites similar to kidney stones,[41] and intrafibrillar mineralization of collagen mimicking the nanostructure of bone[37,42−44]). With this impressive list of replicated features, many of which seem to rely on the fluidic character of the amorphous phase, we have proposed that this process may play a fundamental role in the morphogenesis of biominerals, and can therefore serve as a useful in vitro model system for examining the crystallochemical mechanisms involved.

In our earlier work, we discovered through in situ observations that "transition bars" form during the amorphous to crystalline transformation of the PILP phase.[27] Figure 1 shows the typical appearance of transition bars, which under these conditions are of dimensions that can be readily observed on an optical microscope. The bright-dark bands are quite prominent midway through the transformation, but virtually disappear by the end of the crystallization reaction. Polarized light microscopy (PLM) is a convenient tool for monitoring the progress of the amorphous to crystalline transformation because one can distinguish between amorphous mineral, which is optically isotropic, and its crystalline counterpart, which is birefringent. Use of the gypsum first-order red λ-plate is particularly valuable because it enables both the amorphous and crystalline phases to be observed simultaneously, where the amorphous regions appear as the same magenta color as the isotropic background of the substrate upon which the crystals are grown (i.e., a glass slide or Langmuir monolayer), whereas the crystalline regions exhibit different interference colors (depending on thickness and birefringence), such as orange/yellow and blue in the ∼500 nm thick tablets imaged here (Figure 1B−D).

Figure 1A shows a well-defined transition bar pattern in two single-crystalline tablets of calcite that exhibit a faceted morphology of rhomboidal habit (i.e., a two-dimensional projection consistent with the rhombohedral structure of

(18) Beniash, E.; Aizenberg, J.; Addadi, L.; Weiner, S. *Proc. R. Soc. London, Ser. B* **1997**, *264*, 461–465.
(19) Politi, Y.; Arad, T.; Klein, E.; Weiner, S.; Addadi, L. *Science* **2004**, *306* (5699), 1161–1164.
(20) Raz, S.; Weiner, S.; Addadi, L. *Adv. Mater.* **2000**, *12* (1), 38–42.
(21) Weiner, S.; Levi-Kalisman, Y.; Raz, S.; Addadi, L. *Connect. Tissue Res.* **2003**, *44*, 214–218.
(22) Weiss, I. M.; Tuross, N.; Addadi, L.; Weiner, S. *J. Exp. Zool.* **2002**, *293*, 478–491.
(23) Aizenberg, J.; Hanson, J.; Koetzle, T. F.; Weiner, S.; Addadi, L. *J. Am. Chem. Soc.* **1997**, *119*, 881–886.
(24) Berman, A.; Hanson, J.; Leiserowitz, L.; Koetzle, T. F.; Weiner, S.; Addadi, L. *Science* **1993**, *259*, 776–779.
(25) Albeck, S.; Aizenberg, J.; Addadi, L.; Weiner, S. *J. Am. Chem. Soc.* **1993**, *115*, 11691–11697.
(26) Albeck, S.; Weiner, S.; Addadi, L. *Chem.—Eur. J.* **1996**, *2:3*, 278–284.
(27) Gower, L. B.; Odom, D. J. *J. Cryst. Growth* **2000**, *210:4*, 719–734.
(28) Bolze, J.; Peng, B.; Dingenouts, N.; Panine, P.; Narayanan, T.; Ballauff, M. *Langmuir* **2002**, *18* (22), 8364–8369.
(29) Bolze, J.; Pontoni, D.; Ballauff, M.; Narayanan, T.; Colfen, H. *J. Colloid Interface Sci.* **2004**, *277* (1), 84–94.
(30) Faatz, M.; Grohn, F.; Wegner, G. *Adv. Mater.* **2004**, *16* (12), 996.
(31) Faatz, M.; Grohn, F.; Wegner, G. *Mater. Sci. Eng., C* **2005**, *25* (2), 153–159.
(32) Wohlrab, S.; Colfen, H.; Antonietti, M. *Angew. Chem., Int. Ed.* **2005**, *44* (26), 4087–4092.
(33) Gower, L. A.; Tirrell, D. A. *J. Cryst. Growth* **1998**, *191:12*, 153–160.
(34) Kim, Y.-Y.; Gower, L. B. *Langmuir* **2007**, *23:9*, 4862–4870.
(35) Amos, F. F.; Sharbaugh, D. M.; Talham, D. R.; Gower, L. B.; Fricke, M.; Volkmer, D. *Langmuir* **2006**, *23*, 1988–1994.
(36) Olszta, M.; Gajjeraman, S.; Kaufman, M.; Gower, L. *Chem. Mater.* **2004**, *16:12*, 2355–2362.
(37) Olszta, M. J.; Odom, D. J.; Douglas, E. P.; Gower, L. B. *Connect. Tissue Res.* **2003**, *44* (Suppl. 1), 326–334.
(38) Cheng, X.; Gower, L. B. *Biotechnol. Prog.* **2006**, *22* (1), 141–149.
(39) Patel, V. M.; Sheth, P.; Kurz, A.; Ossenbeck, M.; Shah, D. O.; Gower, L. B. Synthesis of calcium carbonate coated emulsion droplets for drug detoxification. In *Concentrated Dispersions: Theory, Experiments, and Applications*; Markovic, B., Somansundaran, P. ACS Symposium Series 878; American Chemical Society: Washington, DC, 2004; pp 15−25.
(40) Cheng, X.; Varona, P. L.; Olszta, M. J.; Robbins, L. L.; Gower, L. B. *J. Cryst. Growth* **2007**, *307*, 395–404.
(41) Amos, F. F.; Olszta, M. J.; Khan, S. R.; Gower, L. B. Relevance of a Polymer-Induced Liquid-Precursor (PILP) Mineralization Process to Normal and Pathological Biomineralization In *Biomineralization-Medical Aspects of Solubility*; Königsberger, L., Königsberger, L., Eds.; John Wiley & Sons: West Sussex, England, 2006; Chapter 4, pp 125−217.
(42) Olszta, M. J.; Cheng, X.; Jee, S. S.; Kumar, R.; Kim, Y.-Y.; Kaufman, M. J.; Douglas, E. P.; Gower, L. B. *Mater. Sci. Eng., R* **2007**, *58*, 77–116.
(43) Olszta, M. J.; Douglas, E. P.; Gower, L. B. Intrafibrillar mineralization of collagen using a liquid-phase mineral precursor. In *Material Research Society Symposium Proceedings O: Materials Inspired by Biology*, San Francisco, 2003; Thomas, J., Kiick, K., Gower, L., Eds.; MRS: Warrendale, PA, 2003; Vol. 774, pp 127−134.
(44) Olszta, M. J.; Douglas, E. P.; Gower, L. B. *Calcif. Tissue Int.* **2003**, *72* (5), 583–591.

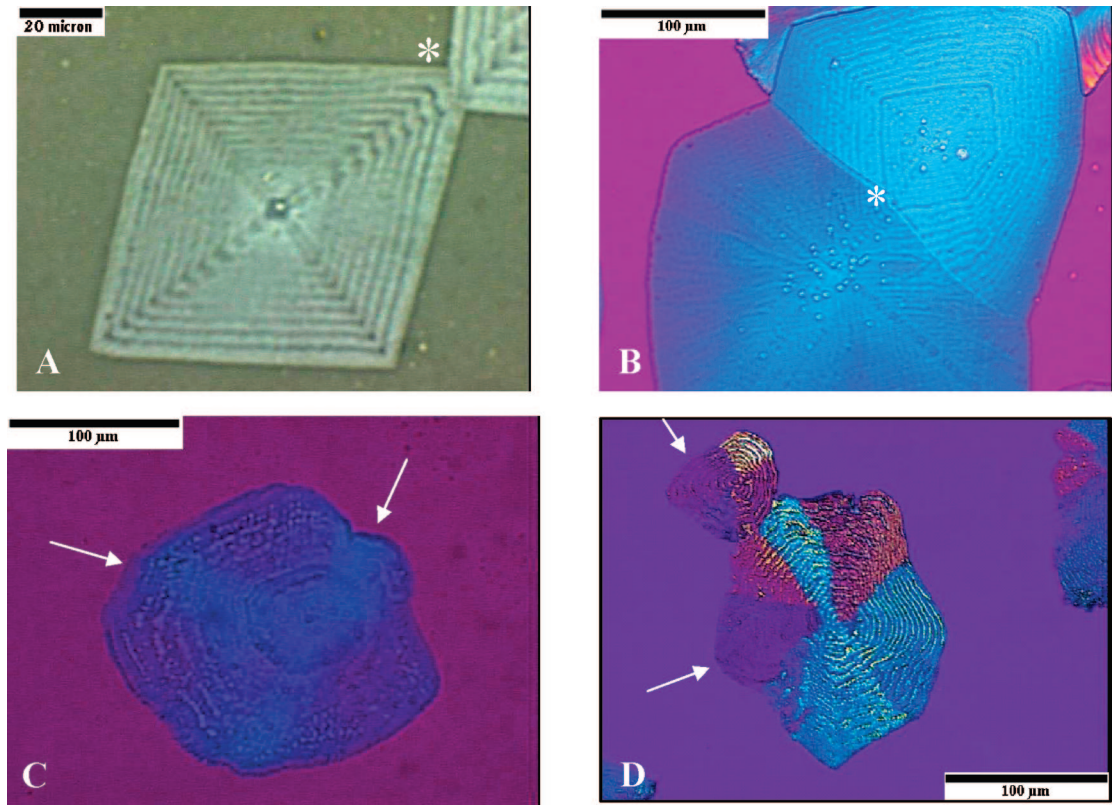

Figure 1. Polarized light micrographs of $CaCO_3$ crystals growing within an ACC film, demonstrating transition bars captured midway through the transformation. Reaction conditions: (A−C) 20 mM $CaCl_2$, 20 μg/mL polyapartate (M_w = 6200), T = 25 °C, deposited on the top glass slide of an in situ crystallization chamber; and (D) 10 mM $CaCO_3$, 6 μg/mL $(PserSD)_6$ polypeptide, deposited under a Langmuir monolayer). (A) Two well-faceted calcite tablets showing pronounced transition bars that are aligned along distinct crystallographic directions. The transition bars divide the tablets into crystallographically delineated sectors (imaged with partially crossed polars; bar = 20 μm. (B) Same two patches of film as in A (imaged at lower magnification, with crossed-polars and gypsum waveplate) have expanded (nearly tripled in size) as the surrounding amorphous film crystallized. The boundaries of the amorphous film cannot be seen since they lie outside the picture. The images are shifted, so the common point is marked with an asterisk. The transition bars in the bottom tablet are nearly gone, and in the top tablet are beginning to diminish. Bar = 100 μm. (C) In this early stage transforming tablet, the transition bars are more pronounced in the less crystalline regions that are still transforming (where isotropic magenta color can be seen between in the bars) and have mostly disappeared in the more crystalline (brighter blue) regions (arrows). Bar = 100 μm. (D) Patch of $CaCO_3$ film composed of differently oriented calcite crystals (exhibiting different interference colors). In this patch, which appears to be transforming from the central region outward, the spacings between transition bars varies among the different sectors of the patch, suggesting that the growth/transformation rate depends on the particular crystallographic direction. This can also be seen in the SEM micrographs in Figure 5C. Bar = 100 μm.

calcite). Figure 1B is of the same tablets (at lower magnification), which have now grown and expanded into larger film patches that impinge upon one another, filling in the preexisting amorphous film (the border of which lies outside the image and therefore cannot be seen in this micrograph). The transition bars in the lower tablet are nearly gone, whereas the transition bars in the upper tablet have diminished but not yet fully disappeared.

In our prior report,[27] it was demonstrated that the transition bars are correlated with the crystallographic lattice, which is fairly obvious in the rhomboidal shaped tablets of Figure 1A. Because of this correlation, the transition bars also divide the "tablets" into crystallographic sectors, which sometimes are rather distorted, as in Figure 1C. In this single-crystalline tablet, the magenta color can be seen within the lighter blue sectors, indicating that these regions have not fully crystallized. The transition bars appear less pronounced in the more crystalline regions (arrows), as would be expected as the bars eventually become filled in with crystalline material. In Figure 1D, the transition bars are very pronounced, except in the less birefringent patches. The originating amorphous film was likely formed at the same time, which suggests that the amorphous-to-crystalline transformation may occur at different rates depending on the crystal growth direction. For example, one can see that the regions with wider bar spacings correspond to regions of greater lateral expansion of the crystalline patch, which overall leads to a nonuniform shape of the crystalline patch. The transition bars in the less birefringent regions (marked with an arrow) are either only just beginning to form, or may have already filled in with crystalline material that lacks birefringence (because of crystal orientation, rather than degree of crystallinity). The greater expansion at the bottom arrow region suggests this was a rapid growth direction, which would then correspond to the latter scenario.

We chose to use the terminology "transition bars" because of their similarity to the transition bars sometimes observed in organic liquid crystals during the isotropic to liquid crystal transition.[45] In liquid crystals, the dark (nonbirefringent) striations are considered a result of the exclusion of impurities, where narrow zones remain isotropic as the impurities

(45) Demus, D.; Richter, L. *Textures of Liquid Crystals*; Verlag Chemie: New York, 1978; p 228.

inhibit the molecular alignment. We suspected that a similar phenomenon might be occurring in our system, where the polymeric additive would be considered an impurity as the amorphous mineral tries to crystallize. Our other studies have shown that a substantial amount of polymer is present in the early stage of PILP formation, which is gradually released as the phase matures, and upon release of the inhibitory polymer, the amorphous phase can then crystallize.[46] However, if not all of the polymer can be excluded to the surrounding aqueous solution, then the only way to exclude the polymer would be to drive it out within the precursor phase ahead of the crystallization front. In a similar system (but not polymer induced), Aizenberg et al.[47] have deposited ACC films in a micropatterned framework and describe a "microsump" function where an incorporated dye became excluded from the growing crystal and concentrated at the posts interfaces of the framework. To determine if a similar phenomenon is responsible for the transition bars in our system, which in this case would consist of exclusion of the polymeric process-directing agent along well-defined crystallographic zones, we labeled the polyaspartate with fluorescein isothiocyanate (FITC) fluorophore, to determine if it collected along the transition bar zones. The specific patterning that results from such an exclusion process could be relevant to features described in the biomineralization literature, as will be explained in the Discussion.

Experimental Section

PILP Crystallization under Langmuir Monolayers via CO_2 Escape Method. Crystallization solutions were prepared with 1.5 g of calcium carbonate powder (Aldrich, 99%) suspended in 500 mL of deionized water, and partially dissolved by bubbling carbon dioxide via a glass pipet at a constant bubbling rate for 24 h. The solutions were then filtered with Whatman filter paper, and the nondissolved calcium carbonate was dried and weighed to determine the dissolved calcium carbonate concentration, which was calculated to be 10 mM. This solution was then filtered with an Acrodisc syringe filter (Gelman Sciences, 13 mm diameter/0.2 mm) prior to usage. An appropriate amount of peptide stock solution (1 mg/ml) was then micropipetted into 10 mL of the calcium carbonate solution contained in a glass dish with a 5 cm internal diameter, to achieve a final concentration of 6 or 15 μg/mL of the polypeptide $(PserSD)_3$ (repetitive amino acids of phosphoserine, serine, and aspartic acid) (synthesis to be described elsewhere).

The surfactant solution was prepared with 8.42 mL of 0.55 mg/mL arachidic acid dissolved in methanol:chloroform (1:9) and was spread onto the air−water interface of the calcium carbonate solution using a 10 μL microliter Hamilton syringe to form a monolayer with a 22 Å^2 calculated surface area per headgroup. The touching of the syringe tip with the water surface was gentle and slow in order to allow full spreading of the arachidic acid to form a uniform monolayer.

The above glass dishes were kept in a Plexiglass chamber placed in an undisturbed place for the mineralization reaction to proceed. After a certain reaction time (which varies over a period of hours to days, depending on type of polymer and ion concentrations, etc.), the reaction products were examined, while still in the Petri dishes, with a polarized optical microscope (Olympus BX-60). The morphology and phase of the final formed minerals were further characterized at high magnification using a JEOL TEM CX200, JEOL SEM 6400, and Nanoscope 3 probe AFM (Digital instruments).

Fluorescence Labeling of Polypeptide. FITC, fluorescein isothiocyanate ($C_{21}H_{11}NO_5S$, M_w = 389.4, Sigma) was used to label the Polyaspartate, the detailed procedure is as follows: For the preparation of 0.1 M sodium carbonate buffer, first 0.2 M sodium carbonate solution was prepared by dissolving 21.2 g of Na_2CO_3 in 1 L H_2O, and 0.2 M sodium bicarbonate was then prepared by dissolving 16.8 g of $NaHCO_3$ in 1 L H_2O. Finally, 8 mL of 0.2 M sodium carbonate, 17 mL of 0.2 M sodium bicarbonate ($NaHCO_3$), and 25 mL of water were mixed. The pH of this buffer solution should be around 9.6. The pH of this solution was then adjusted between 9.1 and 8.3 by adding drops of 0.01 N HCl solution.

For the labeling reaction, two solutions were prepared by dissolving 20 mg of Polymer in 2 mL 0.1 M sodium carbonate buffer and by dissolving 10 mg of FITC in 1 mL DMSO. After that, 200 μL of the above FITC solution was slowly added to the above polymer solution and incubated in the dark at 5 °C for 8 h. To remove the unbound FITC, we used a Centricon YM-3 centrifuge tube (M_w cutoff = 3000 Da) to filter the labeled solution. The retentate conjugate containing the FITC-labeled polymer was stored in a lightproof container in the fridge at 4 °C.

The PILP process using the labeled peptides was performed similarly to that described previously by our group,[27,33] which consists of a modified version of the vapor diffusion method developed by Addadi et al.[48] The polymer used was poly-(α, β)-D,L-aspartic acid·sodium salt (M_w = 8600 unless otherwise specified; Sigma), at concentrations ranging from 2 to 667 μg/mL.

Polarized Light Microscopy (PLM) and Fluorescence Microscopy. The coverslip from each sample was examined using an Olympus BX60 polarized light microscope in transmission mode, using crossed polars and an optional first-order red (gypsum) wavelength plate. The first-order gypsum plate was used primarily to distinguish between amorphous and crystalline phases, in which amorphous phases appear magenta (the same color as the background) while crystalline phases exhibit birefringence and extinction patterns. A calibrated scale bar was put on the digital images using Photoshop software.

For the fluorescence study, a mercury arc lamp was used as a light source and a fluorescence mode NIB filter was chosen. All images from the microscope were acquired digitally (MTI 3CCD camera) by Scion image software (Scion Corporation).

Results

The control reaction, in which free FITC was added to the crystallizing solution, demonstrates that the FITC by itself does not bind in appreciable levels to the calcite crystals, nor does it appear have any noticeable effect on the crystal growth (see the Supporting Information, Figure S1). The calcite still adopted the rhombohedral habit typical of calcite of inorganic origin.

Using a crystal growth chamber that could be mounted under the ultralong-working-distance objectives of a polarizing light microscope (PLM), we were able to monitor the reaction progress in situ and directly observe the progression

(46) Dai, L.; Douglas, E. P.; Gower, L. B. *J. Non-Cryst. Solids* **2008**, *354*, 1845–1854.
(47) Aizenberg, J.; Muller, D. A.; Grazul, J. L.; Hamann, D. R. *Science* **2003**, *299* (5610), 1205–1208.
(48) Addadi, L.; Moradiam, J.; Shay, E.; Maroudas, N. G.; Weiner, S. *Proc. Natl. Acad. Sci., U.S.A.* **1987**, *84*, 2732–2736.

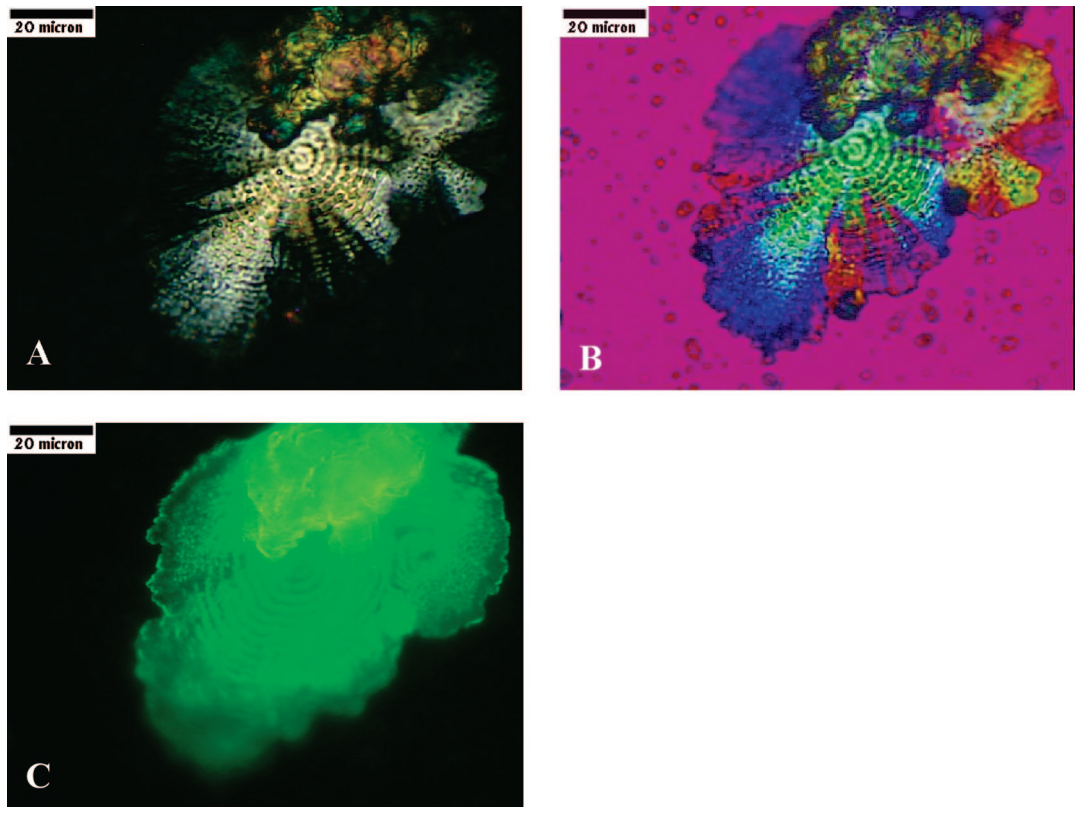

Figure 2. Optical micrographs of a spherulitic patch of $CaCO_3$ film showing the polymer-exclusion phenomenon in the PILP process. (Reaction conditions: 20 mM $CaCl_2$, 111 μg/mL FITC-Pasp additive, 2 days crystallization at $T = 25$ °C). Film imaged with(A) crossed-polarized light and (B) gypsum waveplate; and (C) fluorescence image of same film. The aggregate at the top has intense fluorescence because it is tens of micrometers thick, whereas the film is around 500 nm thick. Scale bars = 20 μm.

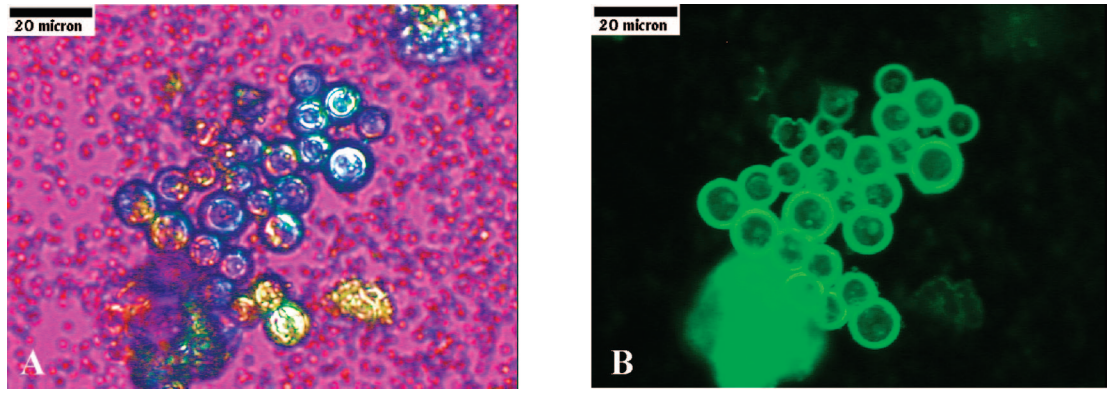

Figure 3. Polymer exclusion phenomenon in spheroidal $CaCO_3$ crystals grown at high polymer concentration. (Reaction conditions: 20 mM $CaCl_2$, 666 μg/mL FITC-Pasp, 2 days vapor diffusion at $T = 25$ °C). (A) Polarized light with gypsum waveplate shows large spheroidal particles that do not appear to be spherulites because they lack a Maltese cross pattern. The multitude of micrometer-sized particles surrounding these are more typical of the dimensions seen for PILP droplets. (B) Fluorescence image shows that these large particles have a core−shell texture, with a pronounced enrichment of polymer in the shell. Scale bars = 20 μm.

of the transition bars. As can be seen by the polymer-enriched and polymer-poor zones in the fluorescence image in Figure 2, the labeled polymer follows the same pattern as the transition bars, indicating that these are indeed a result of polymer exclusion (see the Supporting Information, Figure S2, for a higher-magnification view). In this case, the patch of film is spherulitic (which in our prior studies were found to be the vaterite phase[33]), and the impurity is excluded in incremental steps along the radial growth direction. The fact that similarly spaced transition bars appear in both spherulitic and single-crystalline mineral films suggests that the spacing of these bars is due to diffusional limitations, in which polymer ultimately gets entrapped within the film as it becomes too solidified for the large polymer to be driven out.

A striking example of the polymer-exclusion phenomena is shown in Figure 3, in which a higher polymer concentration led to some large spheroidal particles of $CaCO_3$ (Figure 3A). Fluorescence microscopy shows that these globules had crystallized into core−shell particles, where the labeled polymer is clearly seen to be enriched in the shell region (Figure 3B). Given the relatively large size of the spheroidal particles (which are not spherulites, as seen by the lack of a Maltese cross pattern), it seems the mobility of the polymer must have been quite high

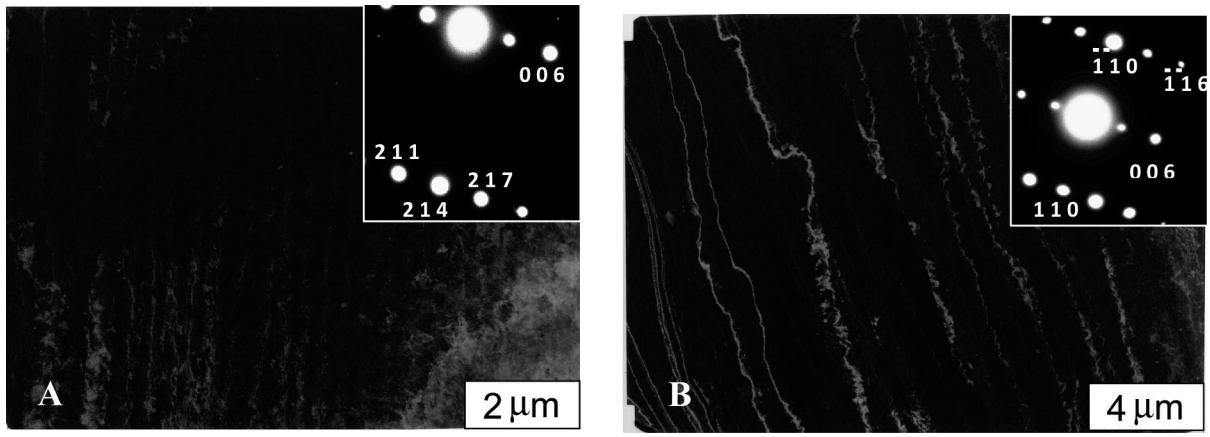

Figure 4. TEM images and SAED patterns of $CaCO_3$ films formed underneath Langmuir monolayers of arachidic acid, using 15 μg/ml of $(DEPser)_3D$ polypeptide (3 days of reaction). A) A relatively smooth region of film with narrow aligned striations. (B) Wider and more pronounced striations that appear to be ridges. Both regions show single-crystalline SAED spot patterns that match the *d*-spacings of calcite. Indices are based on JCPDS 05−0586 for biogenic calcite.

to yield such a pronounced accumulation of polymer, suggesting that the originating spheroidal globules had a fairly fluidic precursor. Our prior work on helical vaterites showed that the shell regions have a very fine spherulitic texture (as seen by SEM),[33] which in light of these studies might be expected because of the inhibitory effect of the excess polymeric impurity in those regions.

The transition bars are not always linear, and often appear to follow the distortions in the overall shape of the crystal (e.g., Figure 1C & D). A high degree of curvature can be seen in crystals that otherwise appear to be single crystalline (exhibit uniform extinction direction), and even in the SEM images of Figure 5. We believe this is indicative of distortions in the internal lattice structure of the crystal due to dehydration stresses. This is suggested on the basis of observations of single crystals that exhibit a gradually shifting birefringence which becomes more pronounced the farther the growth front moves from the point of nucleation; and crystal overgrowths on such films present facets that shift in orientation in a pattern consistent with biaxial film strain.[27]

The distortions are variable for different sectors, which may be related to different growth rates (and therefore dehydration rates) along different crystallographic directions. The polymer additive could confound this situation through preferential binding to different step edges. For example, selective binding has been demonstrated in conventional solution crystallization experiments, where researchers have monitored spiral growth hillocks with AFM and find that impurities bind selectively to different growth steps, leading to pronounced distortion of those growth steps (and corresponding crystal morphology).[49,50] The AFM images of those step edges look quite similar to the transition bars seen here, even though they are imaged at very different size scales (AFM of molecular growth hillocks versus micrometer-size optical features in flat films). This is because both features, atomic step edges and transition bars, are correlated with the crystal growth direction. For example, if one carefully examines the rhomboidal PILP tablet in Figure 1A, the transition bars can be seen to follow a spiral growth pattern. Spiral growth hillocks are commonly observed for calcite grown from solution, so it seems reasonable that this growth mechanism might also occur for crystals growing from the amorphous phase. However, the conditions here are far from equilibrium, so unusual growth morphologies result. For example, each birefringent bar would have to correspond to numerous rounds of spiral growth that apparently keep pushing aside the polymeric impurity until it accumulates in the isotropic zones. The spiral appears to be continuously connected; therefore, it seems that some type of step bunching is responsible for this "macrostep" formation. Such morphological instabilities are observed for crystal growth subjected to diffusional constraints (or latent heat in the case of melts);[51] but here, it is not clear if this is due to diffusion of solute in, or diffusion of polymer out, of the crystallization front.

Different textures can be found for the transition bars, as seen in the TEM images of Figure 4 and the PLM and SEM images of Figure 5. Transition bars are not always observed, which in large part is due to the inability to observe the reaction midway, and little evidence of these bars remains in the final crystalline films. On the other hand, it also may depend on the dimensions of the diffusion limited zones. For example, the TEM micrographs in Figure 4 show aligned striations that appear to be related to transition bars, but in this case, the periodicity is so small that it would not be easily detected on the optical microscope. These films were grown under a Langmuir monolayer of arachidic acid, which made them easy to retrieve for TEM analysis. The single-crystalline spot pattern obtained by selected area electron diffraction (SAED; inset) further illustrates that these anisotropic textures can occur in single-crystalline calcite with no appreciable disruption of the lattice pattern.

There appears to be substantial variability in the texture of transition bars, which not only depends on the reaction conditions, but can also depend on the characteristics of the polymeric process-directing agent. For example, variability

(49) Orme, C. A.; Noy, A.; Wierzbicki, A.; McBride, M. T.; Grantham, M.; Teng, H. H.; Dove, P. M.; DeYoreo, J. J. *Nature* **2001**, *411* (June), 775–779.

(50) Teng, H. H.; Dove, P. M.; DeYoreo, J. J. *Geochim. Cosmochim. Acta* **1999**, *63:17*, 2507–2512.

(51) Potapenko, S. Y. *J. Cryst. Growth* **1995**, *147* (1−2), 223–233.

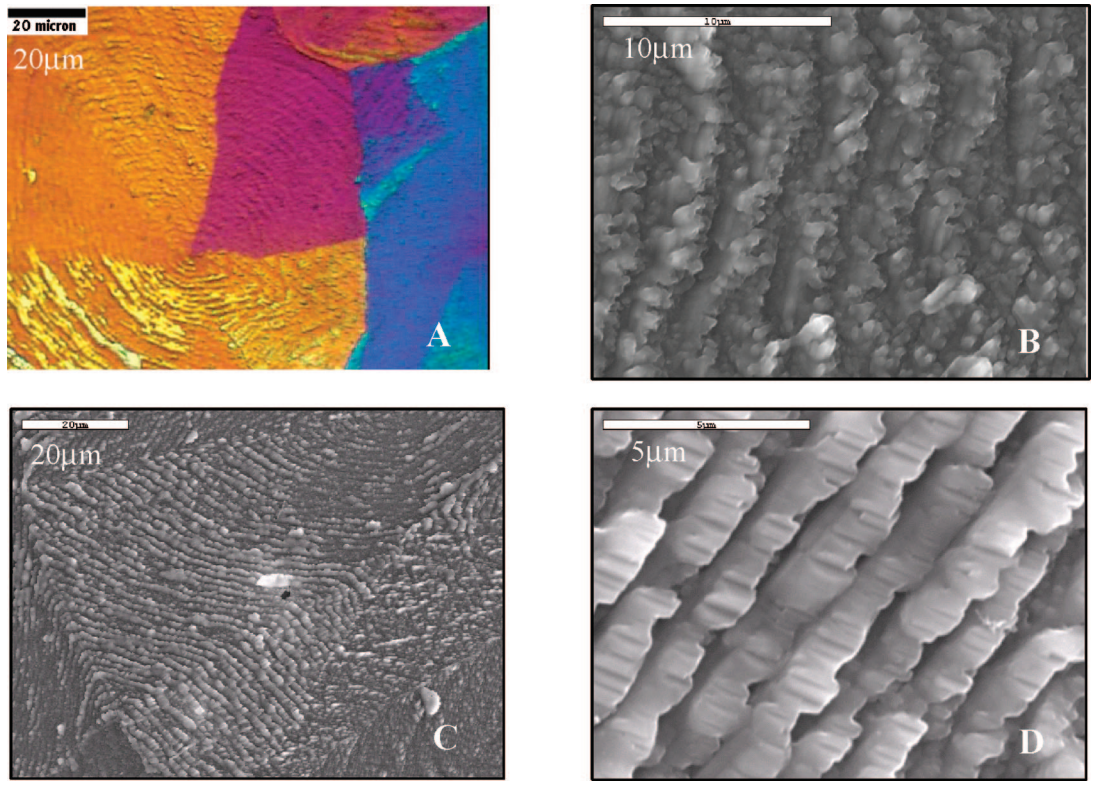

Figure 5. Transition bar topography study of a $CaCO_3$ film deposited from 15 μg/mL $(PserSD)_6$ peptide under a Langmuir monolayer of arachidic acid. (A) Mosaic film imaged with polarized light microscopy using the gypsum λ-plate, showing both relatively smooth regions and ridgelike regions, the texture of which appear to depend on the crystal growth direction. In the lower left corner, the transition bars are widening and beginning to coalesce and smooth out, forming a new thicker layer (indicated by the higher-order yellow retardation color). (B) SEM micrograph of a relatively smooth region of a film showing undulatory "waves" of mineral. The somewhat granular morphology of the ridges may be due to adsorption of nanoscale droplets of PILP phase. (C) SEM micrograph of a region with well-aligned "sawtooth" ridges, which is further magnified in (D). The mineral bands appear to have further broken down into a subset of bands orthogonal to the primary bands. In (C), variability in the spacing and topography can be seen along the different crystallographic directions (best viewed by zooming in on the electronic version).

in the amount and texture of transition bars was seen for a series of polypeptides that mimic the domains of biomineralization proteins, such as osteopontin and phosphophoryn (publication in preparation). For example, transition bars were frequently observed in the films generated by a $(PserSD)_3$ peptide (repetitive amino acids of phosphoserine, serine, and aspartic acid), which mimics the acidic domains of phosphophoryn. The films were not always flat because of a nonuniform accumulation of PILP phase, and often had a thick "skeletal" ridge running down the middle, where the bars were often more prominent in the thicker regions of film (see the Supporting Information, Figure S3, and the Table of Contents graphic). This might be due to the longer diffusion path to the surface of the film, where in a thin film, the polymer could be more readily released at the surface.

As might be expected, the presence of transition bars is also a function of polymer concentration. For example, two different concentration levels of the $(PserSD)_3$ peptide showed differences, where transition bars were only observed in the 15 μg/mL peptide induced films, and not at 6 μg/mL (the films were also less continuous and not as good in quality as the higher peptide concentration). Transition bars were recognizable during the first 6 days of reaction; after this, the undulations in birefringence were "smoothed out". It was not clear if this is an optical effect, or if there are truly topographical ridges present. In other words, the dark "valleys" may only be nonbirefringent amorphous bars surrounded by birefringent crystalline "ridges", even though the overall surface may be flat and smooth, defined by the thickness of the initially amorphous precursor film.

This peptide system showed some intriguing results for the transition bars, which may further contribute to an understanding of the phenomenon. At a concentration of 15 μg/mL, $(PserSD)_6$ induces nice continuous films with parallel ridges easily identified as transition bars. In some regions of the crystalline films, the transition bars are less separated and appear to be coalescing into thicker patches (Figure 5A, bottom left corner). The higher-order retardation color (yellow) indicates that the transition bars are thicker than the surrounding orange layer (or blue layer in Figure 1D, which also has thicker yellow ridges). These types of films were collected for examination by scanning electron microscopy (SEM), which reveals a distinct variability in the film topography, ranging from undulatory "ripples" (Figure 5B) to pronounced "ridges" (C and D in Figure 5). Figure 5C is an SEM image of a region with well-aligned ridges, which is magnified in Figure 5D, and shows a highly pronounced 'sawtooth' pattern. Similarly, the AFM image in Figure 6A also shows the 3-dimensionality and alignment of these ridges. The thickness of the crystalline films is around 600 nm, as determined by the AFM image of a film edge shown in Figure 6B.

In our previous studies of $CaCO_3$ films deposited on glass (and in Figure 1A−C here), it seemed as though the undulatory birefringence was an optical effect (and not

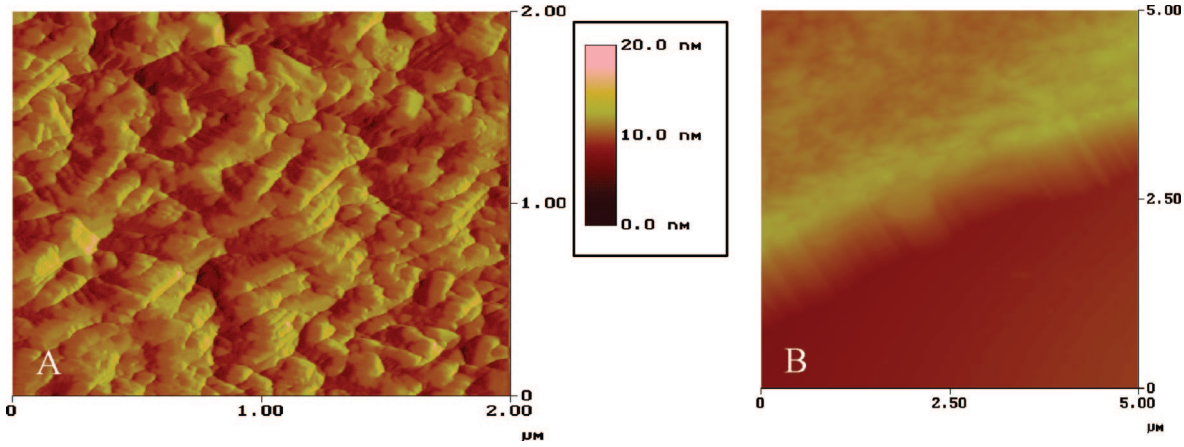

Figure 6. Atomic force microscopy (AFM) of $CaCO_3$ film prepared with $(PserSD)_6$ additive under a Langmuir monolayer of arachidic acid. The *x*/*y*-axes are 2 μm; *z*-scale (inset) to 20 nm. (A) AFM images show alignment of the transition bar ridges which appear similar to the SEM images of the "sawtooth" ridges. (B) AFM measurement of the thickness of the film edge, which is around 600 nm.

physical ridges). This does not appear to be the case for the films extracted from Langmuir monolayers, which at the midpoint of these reactions are clearly not smooth (Figure 5). This may be related to the fact that these films were formed on a flexible organic monolayer, instead of glass, which could allow "wrinkling" of the films as they shrink during dehydration and crystallization. We do not believe this to be the case though, because the ridges "anneal" with time to become smooth and continuous films. This then begs the question, how do the films end up with a smooth surface at the completion of the reaction?

One possible explanation is that transformation of the amorphous precursor proceeds through a dissolution/recrystallization route; but smooth films would not be expected in this case because the films consist of variously oriented calcite crystals with surfaces that do not expose the planes of lowest free energy (they expose whichever plane nucleates on the substrate because they are constrained to grow within the phase boundary of the amorphous precursor film). Instead, one would expect recrystallization to lead to microfacets of the (104) planes to give the lowest surface energy (as is seen for crystal overgrowths on such films[27,52]). Therefore, we suspect that the "annealing" effect may be caused by a second round of PILP droplets, which are locally induced by the polymer that has been excluded to the transition bar regions, such that new PILP phase could fill in the ridge patterns to make smooth films. We have observed that PILP droplets like to adsorb to defects and edges of preformed films,[53,54] so it would be reasonable to expect them to accrete and fill-in these high-energy ridged regions to minimize the surface area, in a "wetting" type of deposition process. In this case, because the PILP phase is still in the amorphous isotropic state, it would not yield anisotropic surface energies to create microfacets. An illustration depicting this proposed mechanism of transition bar formation and "annealing" is provided in Figure 7.

An annealing effect has also been described by Sethman et al.,[55] who examined the transformation of a "gelatinous" mineral precursor (also induced with polyAsp) that was deposited on calcite substrates. In situ AFM showed that faceted polycrystals emerged from the calcite substrate via homoepitactic nucleation, which subsequently "fused" into semicoherent domains (the mechanism of fusion was not determined). Their system seems quite similar to ours, with the main difference being the calcitic substrate, which stimulates rapid secondary overgrowths via epitaxy, instead of the more random and less prevalent nucleation events in our system. But in both cases, the emergence of the crystal phase from an amorphous precursor seems to yield interesting nanostructures that somehow manage to resolve into smooth structures, and quite possibly from filling in the interstices with further doses of precursor phase.

In summary, these studies demonstrate that transition bars are a result of exclusion of polymeric impurity to diffusion-limited and crystallographically delineated zones. We cannot say for certain that all transition bars have this three-dimensionality of ripples; nor can we say that all ACC, or even PILP film transformations, contain transition bars. But it is clear that certain variables influence these factors, such as the type of polymer (e.g., charge density, molecular weight) and concentration of polymer, both of which probably influence the degree of hydration of the PILP phase and its solidification rate. The substrate is also thought to influence how quickly the amorphous phase solidifies, as well as other conditions not examined in detail here, such as concentration of reactants, stoichiometry of reactants, other impurities (e.g., Mg ion), and temperature.

(52) Volkmer, D.; Harms, M.; Gower, L.; Ziegler, A. *Angew. Chem. Int. Ed* **2005**, *44*, 639–644.
(53) Kim, Y.-y. Patterning of Bioinorganic Thin Films by Combining Soft Lithography and a Biomimetic Crystallization Process. Dissertation, University of Florida, Gainesville, FL, 2003.
(54) Kim, Y.-Y.; Gower, L. B. Formation of complex non-equilibrium morphologies of calcite via biomimetic processing. In Materials Research Society Symposium Proceedings, San Francisco, 2003 Material Research Society Symposium Proceedings O: Materials Inspired by Biology, San Francisco, 2003; Thomas, J., Kiick, K., Gower, L., Eds.; MRS: Warrendale, PA, 2003; Vol. 774.
(55) Sethmann, I.; Putnis, A.; Grassmann, O.; Lobmann, P. *Am. Mineral.* **2005**, *90*, 1213–1217.

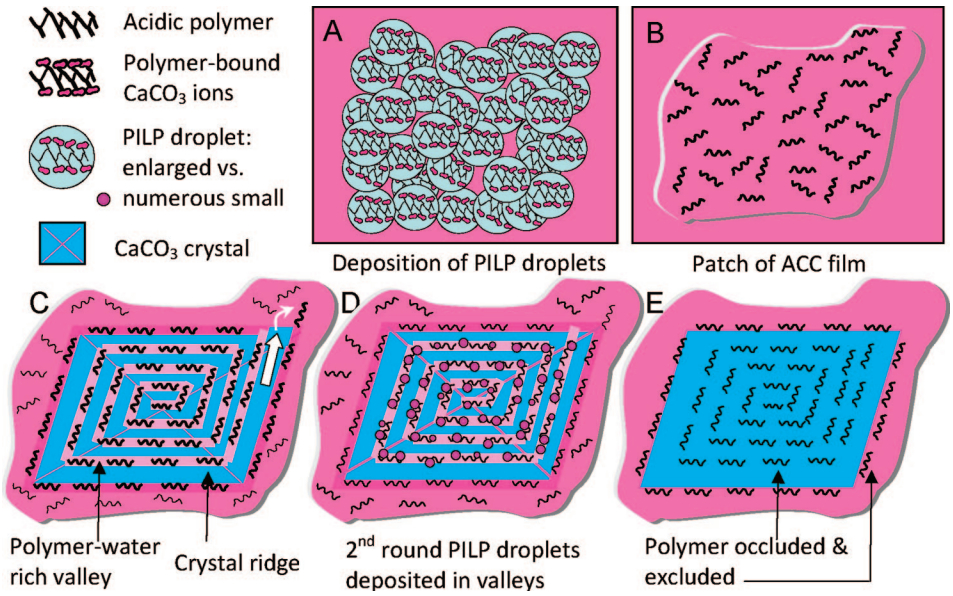

Figure 7. Schematic depicting the proposed mechanism involved in the formation and "annealing" of transition bars during the amorphous-to-crystalline transformation of a PILP mineral precursor. (A) Acidic polymer sequesters ions or clusters of $CaCO_3$ to form PILP droplets which deposit randomly on a substrate (e.g., a Langmuir monolayer or glass). This view of the PILP droplets is enlarged relative to the rest of the series. (B) Precursor droplets coalesce to form a smooth and continuous amorphous film that has entrapped some of the polymer. (C) As the amorphous phase tries to crystallize, polymer and water are excluded; but as the PILP phase solidifies, the diffusion of the polymer that is being pushed aside becomes limited, leaving behind traces of the polymeric impurity that become entrapped in the transition bars, which remain amorphous (nonbirefringent) because of the inhibitory effect of the polymer. The white arrow indicates the lateral crystal growth direction, along with polymer being rejected to the side. A substantial amount of water may also be excluded from the crystallization front, thus leading to the topographical features of ridges and valleys. (D) Secondary round of PILP droplets may be deposited preferentially at the high-energy sites, such as the edges of the transition bars. This secondary deposition might also be surface induced by the locally high concentration of excluded polymer in the bar regions. (E) Valleys become filled in because of the wetting behavior of the fluidic precursor (rather than forming a conformal coating over the ridges), leading to a smooth and continuous crystalline film. Some polymer becomes occluded within the crystal along well-defined crystallographic zones, along with some remnant polymer at the surface of the crystal, which in the case of biomineral formation, would be overlaid by sequential deposits of mineral, leading to selective occlusion of polymer along specific crystallographic zones, as well as between the layers of sequential deposition (leading to concentric "growth rings"), respectively.

Discussion

Banded Crystal Growth. Banded crystal growth patterns can be found in a variety of materials, ranging from metal alloys to paraffins. For example, in metals, constitutional supercooling can occur during the directional solidification of a melt, which leads to fingerlike projections orthogonal to the growth interface.[56] This results from the build-up of impurities at the solid−liquid interface, which becomes thermodynamically unstable such that a small perturbation breaks down into a wave of projections that reject the impurities to the sides as they lengthen. Crystallization in metals often proceeds via growth normal to the growth interface, so that when the impurities are rejected laterally, the bands (called cellular protrusions) are orthogonal to the growth front. The opposite pattern seems to occur in the PILP system. This may be because crystal growth proceeds laterally for calcite (parallel to the growth interface), as is suggested by the spiral growth pattern of the transition bars mentioned earlier. Therefore, as calcite growth proceeds laterally, the rejection of impurities in the PILP system (polymer pushed to the side) leads to bands that run parallel to the macroscopic growth interface (expressed crystal faces), even though the bands are perpendicular to the actual growth direction at the atomic level. Likewise, the spherulitic films have similarly spaced transition bars in the radial growth direction, but they do not spiral because lateral growth is occurring within each of the individual polycrystals. In contrast to metals, there is no evidence in the PILP system to suggest that the banding is thermodynamically controlled (such as the cellular breakdown seen in metals), and instead the diffusional constraints of this system seem more likely to be responsible for a kinetically hindered growth process.

The crystallization of *n*-alkanes in the presence of impurities (kinetic inhibitors) leads to banding patterns that are even more similar in appearance to the PILP system because the bands are parallel to the macroscopic growth interface. Hutter et al.[57] have examined the crystallization of tricosane (n-$C_{23}H_{48}$) in dodecane solution under a thermal gradient, and when crystallized in the presence of poly(octadecyl acrylate) inhibitor, the growth front forms a series of nearly unconnected bands parallel to the front, with a periodicity of several hundred micrometers. They suggest that the inhibitor produces a "dead zone", in which a minimum supersaturation is needed for growth to proceed. However, nucleation of a new solid domain can occur in the supersaturated region ahead of the dead zone. The new band then spreads laterally, limited by high temperature on one side and solute depletion on the other. This band creates its own depletion zone and the cycle repeats. Their results show that the band wavelength generally decreases with increasing C23 concentration, and is a decreasing function of the imposed velocity. Because banded growth was never seen in the absence of inhibitor,

(56) Davis, S. H. *Theory of Solidication*; Cambridge University Press: Cambridge, 2001; p 385.

(57) Hutter, J. L.; Hudson, S.; Smith, C.; Tetervak, A.; Zhang, J. H. *J. Cryst. Growth* **2004**, *273* (1−2), 292–302.

even at much higher velocities, it was concluded that the activity of this inhibitor must be important in the banding mechanism.

The PILP system does not employ a thermal gradient to drive the crystallization reaction; nevertheless, it seems likely the mechanism for banding is related with respect to generating "dead zones", which in the PILP system would arise from a combination of solute depletion and excessive inhibition caused by the enriched polymer in these zones. The velocity effect described by Hutter also seems relevant to the PILP system, but rather than observing a relationship with solute concentration or temperature, which are not controlled variables in our system, the variability in band spacing seems to depend on the crystal growth direction (which would inherently provide different growth velocities).

In the $CaCO_3$ PILP system, where ACC is considered a highly unstable phase, the driving force for crystallization should be very strong. However, the polymeric additive is not as easily transported by diffusion, therefore, the presence of these banding patterns, where the fluorescently labeled polymer clearly has been transported during the crystallization process, may be providing an indicator of the fluidic character of the precursor phase. Our previous in situ synchrotron X-ray reflectivity studies show that the $CaCO_3$ films deposited under Langmuir monolayers are quite hydrated, with an electron density of 70% the hexahydrate phase.[58] Likewise, the thicker film deposits have more pronounced banding, which we believe may be due to a higher degree of fluidity (the thin films seem to solidify rapidly when contacting a substrate). In the case of the alkanes, the periodicity of the banding patterns is on the order of several hundred of micrometers, whereas in the PILP system, the bands are only micrometers in spacing (or smaller, as seen in Figure 4A). Although the polymer in the amorphous $CaCO_3$ phase is apparently less mobile than in the polymer in the alkane solution, it certainly does not seem to be immobilized in a solid ACC phase. We are not aware of any literature dealing with mineral precipitation reactions from solution that show banding patterns such as these, and therefore conclude that the unique characteristics of the PILP amorphous precursor phase, with limited but not prohibitive diffusive transport of the inhibitor, is responsible.

Relevance to Biomineralization. The concept of stereoselective adsorption has been at the forefront of biomineral and biomimetics research for around 20 years. However, with the recent evidence of a transient amorphous phase in echinoderms (urchins and sea stars) and mollusks,[2,17−22] this concept of specific interactions and selective adsorption has come under scrutiny. It is not clear how these proteins would play a role in the morphogenesis of biominerals whose shapes are already "molded" by the biological compartments in which the amorphous mineral precursor is deposited. This is not meant to imply that such interactions cannot modulate crystal growth. Indeed, the use of additives for modifying crystal growth through specific crystal-additive binding interactions has been widely utilized by industry for a variety of commercial applications. It is just no longer clear how such interactions might be involved in biomineralization.

The studies presented here may shed some light on the earlier reports in the literature regarding stereoselective adsorption of proteins in biomineralization.[9,13,14,16] In vitro crystallization assays using proteins extracted from the spines of sea urchins suggested that the proteins specifically bind to different crystallographic planes,[25,26] as evidenced by the expression of a new {10*l*} set of crystal faces. Proteins were occluded within the final crystals as determined by quantitative amino acid analysis.[23] In support of this claim, ex vivo synchrotron X-ray diffraction studies of biological specimens showed anisotropic defect texture of the urchin spine,[23,24] suggesting an anisotropic distribution of proteins along select crystallographic directions within the biomineral.

Based on the observations of transition bars, we propose that the anisotropic distribution of proteins within biominerals may result from the anisotropy of polymer *exclusion* during the precursor transformation stage, rather than anisotropic *inclusion* of the proteins via stereospecific adsorption. During the restructuring of the amorphous phase, the polymer exclusion from the growth front leads to anisotropic inclusions, which appear to be affected by the kinetics of crystal growth in different directions. For example, the fast growth directions may push through the impurities and leave them behind to settle onto the more stable crystallographic faces, leading to a polymer distribution that differs for each family of crystallographic growth directions.

During the amorphous to crystalline transformation, the polymer could be excluded from the growing crystal by a variety of pathways, which would depend in large part on the thickness of the deposited mineral, as well as its solidification rate (assuming the biomineral is formed by the PILP process). Much of the impurities may be fully removed from the crystals and dissolve back into the aqueous phase, (as is the case in our model system[46]), or perhaps some of the protein may remain in the vicinity of the crystal surface, leaving behind layers of organic matrix interspersed between the crystals (perhaps as the thin membranes surrounding nacreous tablets,[59−63] or the concentric laminations seen in urchin spines, sea sponges, and a variety of other biominerals),[25,64] and finally as a minor component that becomes

(58) DiMasi, E.; Patel, V. M.; Sivakumar, M.; Olszta, M. J.; Yang, Y. P.; Gower, L. B. *Langmuir* **2002**, *18* (23), 8902–8909.

(59) Nakahara, H. Nacre formation in bivalve and gastropod molluscs. In *Mechanisms and Phylogeny of Mineralization in Biological Systems*; Suga, S., Nakahara, H., Eds.; Springer: Tokyo, 1991; pp 343−350.

(60) Smith, B. L.; Schaffer, T. E.; Viani, M.; Thompson, J. B.; Frederick, N. A.; Kindt, J.; Belcher, A.; Stucky, G. D.; Morse, D. E.; Hansma, P. K. *Nature* **1999**, *399*, 761–763.

(61) Schaffer, T. E.; Ionescu-Zanetti, C.; Proksch, R.; Fritz, M.; Walters, D. A.; Almqvist, N.; Zaremba, C. M.; Belcher, A. M.; Smith, B. L.; Stucky, G. D.; Morse, D. E.; Hansma, P. K. *Chem. Mater.* **1997**, *9:8*, 1731–1740.

(62) Nakahara, H. Nacre formation in bivalve and gastropod molluscs. In *Biomineralization '90*; Springer-Verlag: New York, 1991; pp 343−350.

(63) Fantner, G. E.; Oroudjev, E.; Schitter, G.; Golde, L. S.; Thurner, P.; Finch, M. M.; Turner, P.; Gutsmann, T.; Morse, D. E.; Hansma, H.; Hansma, P. K. Sacrificial bonds and hidden length: Unraveling molecular mesostructures in tough materials. *Biophys. J.* **2006**, *90* (4), 1411–1418.

(64) Sethmann, I.; Wörheide, G. *Micron* **2008**, *39* (3), 209–228.

occluded within the crystals, preferentially enriched in the crystallographically defined transition bar zones.

Another consideration is that although there are distinct differences between conventional crystal growth versus crystal transformation via an ACC precursor, there may be analogous organic−inorganic interfacial interactions that play a role in each. For example, the in situ crystal growth studies with AFM, which are typically designed for the purpose of understanding crystal shape modulation, have shown that the preferential adsorption of additives is correlated with the geometry of the growing step edges, and not with flat crystal planes.[50,65,66] In the PILP system, it is possible, and likely, that the entrapped proteins will have a different affinity for the different crystal faces or growth steps that form during the amorphous to crystalline transformation, and therefore alteration of the kinetics of the crystal growth based on the directionality of these affinities with certain crystal planes might be expected. This of course sounds similar to the former hypothesis of selective adsorption.[13−15] However, this preferential partitioning would primarily influence the location of the occluded proteins, rather than dictate the overall morphology of the biomineral (although it may influence which edges of a tablet are expressed; indeed, a variety of tablet shapes are seen in nacre, from round to well-faceted[62]). In other words, the data indicating a preferential occlusion of proteins was not necessarily just a coincidence; but the reason behind this selective occlusion, which was interpreted as being related to selective adsorption of proteins, may have been due to selective exclusion of proteins, and thus not as relevant to the regulation of crystal morphology.

In a related example, sectorization patterns have been observed in the aragonite and calcite tablets of nacre (mollusks)[1] and seminacre (bryozoans),[67] which has been attributed to selective protein binding in those particular sectors.[14] Again, the sectorization phenomenon shown here could offer an explanation for the biogenic sectorization patterns. The narrower sectors of the hexagonal tablets in seminacre were observed to have preferential etching, which as described in our prior report,[27] correlate nicely with the higher defect texture seen in the narrower sectors of our pseudohexagonal "tablets" of calcite. One would expect sectors that are enriched with impurity to suffer more deterioration and etching.

Although we suggest that protein adsorption to specific crystallographic faces is not necessarily responsible for regulation of biomineral morphology, selective protein exclusion may still be one of Mother Nature's tools for regulating the mechanical properties the biomineral composites. In fact, proteins may have evolved with specificity of exclusion/occlusion to create more durable bioceramic structures. For example, the fenestrated echinoderm skeleton reportedly has an excellent strength-to-weight ratio, with a crushing strength comparable to the strength of polycrystalline mollusk shells and limestones of high bulk density.[8] The occluded proteins,[6,68] magnesium impurities,[8] and/or lattice stress/strain[4,69] could all influence these properties. Lastly, it should be remembered that the soluble proteins could be multifunctional and serve a variety of other regulatory functions other than modulation of crystal morphology and texture, such as control of crystal phase and orientation (or biochemical functions).

As is always the case, caution should be exercised when trying to draw conclusions from ex vivo evidence, and of course, the same can be said for in vitro evidence (as is the case here). Neither is as convincing as in vivo evidence, but this is usually very difficult to obtain when it comes to studying the formation of hard tissues. We believe the best approach is to use a combination of these methods, such as analysis of ex vivo features to identify novel features of interest, and in vitro model systems to develop an understanding of the crystallochemical mechanisms involved in producing those types of features. Neither one should be overlooked, because this approach can contribute valuable insight into materials processing.

Conclusions

Transition bars have been monitored in situ during the amorphous to crystalline transformation of ACC films deposited under Langmuir monolayers and on glass slides via the polymer-induced liquid-precursor (PILP) process. The transition bars have been produced under several different reaction conditions, yielding an assortment of textures and periodic increments, which may be related to the degree of hydration (fluidic character) of the precursor. Optical microscopy was used to examine the amorphous to crystalline transformation in situ. SEM and AFM demonstrated the three-dimensional nature of the transition bar ridges. TEM found striated textures within single crystalline regions of film. Fluorescence microscopy demonstrated that the transition bars are a result of diffusion-limited exclusion of the polymeric impurity, part of which becomes preferentially entrapped within well-defined crystallographic zones of the crystals, and part of which may be at the surface and stimulate further deposition of precursor phase to fill in the valleys and smooth out the films.

The sectorization of tablets and crystallographic anisotropy of the polymer occlusions in the PILP system may help to explain some of the crystal textures found by ex vivo analysis of biominerals, which also exhibit sectorization patterns (nacre and seminacre), concentrically laminated composites, and planes of preferential occlusion of proteins within biomineral crystals. In conclusion, in addition to the ability to reproduce a variety of morphological features found in biominerals, the PILP process also seems to produce certain crystallographic textures found in biominerals; therefore, these findings continue to support the hypothesis put forth by our group that the PILP process may play a fundamental role in biomineralization.

(65) Teng, H. H.; Dove, P. M.; Orme, C. A.; DeYoreo, J. J. *Science* **1998**, *282*, 724–727.
(66) Teng, H. H.; Dove, P. M.; Yoreo, J. J. D. *Geochim. Cosmochim. Acta* **2000**, *64:13*, 2255–2266.
(67) Weedon, M. J.; Taylor, P. D. *Biol. Bull.* **1995**, *188*, 281–292.
(68) Berman, A.; Addadi, L.; Kvick, A.; Leiserowitz, L.; Nelson, M.; Weiner, S. *Science* **1990**, *250* (4981), 664–667.
(69) Zolotoyabko, E.; Pokroy, B. *CrystEngComm* **2007**, *9:12*, 1156–1161.

Acknowledgment. We appreciate the insightful discussions with Martin Glicksman and Jim DeYoreo. Financial support provided by the National Science Foundation (Grant DMR-0094209), and in part by NASA (Grant NRA 00-OSS-01-043), is gratefully acknowledged. We also thank the Major Analytic Instrumentation Center (MAIC) of the University of Florida for maintaining and providing exceptional analytical equipment and guidance for the SEM, TEM, and diffraction analysis.

Supporting Information Available: Three additional figures showing (1) the nonmodulatory effect of the fluorophore on the growth of calcite rhombs, (2) a higher-magnification fluorescence image of the transition bars, and (3) the prevalence of transition bars in thicker films. This material is available free of charge via the Internet at http://pubs.acs.org.

CM800760P